Marine Environmental Research 188 (2023) 105975

Contents lists available at ScienceDirect

Marine Environmental Research

journal homepage: www.elsevier.com/locate/marenvrev

Vertical distribution of inorganic nanoparticles in a Norwegian fjord

Are S. Bruvold [a,b,*], André Marcel Bienfait [a], Torunn Kringlen Ervik [c], Katrin Loeschner [d], Stig Valdersnes [a,b]

[a] Institute of Marine Research, P.O. Box 1870 Nordnes, NO-5817, Bergen, Norway
[b] University of Bergen, Department of Chemistry, P.O. Box 7803, N-5020, Bergen, Norway
[c] Norwegian Institute of Occupational Health, P.O. Box 5330, Majorstuen, 0304, Oslo, Norway
[d] National Food Institute, Technical University of Denmark, Kemitorvet 201, DK-2800, Kgs, Lyngby, Denmark

ARTICLE INFO

Keywords:
Nanoparticles
Colloids
Fjord
SP-ICP-MS
Metals
Sampling
Seawater
Coast

ABSTRACT

Due to the analytical challenges of detecting and quantifying nanoparticles in seawater, the data on distributions of NPs in the marine environment is limited to qualitative studies or by ensemble measurements subject to various analytical artifacts. Single particle inductively coupled plasma mass spectrometry (SP-ICP-MS) allows determination of individual inorganic NPs at environmentally relevant concentrations, yet only few studies have been conducted on selected elements in surface sea water. Here, a sequential multi-element screening method was developed and implemented to provide a first survey of the horizontal and vertical distributions of inorganic nanoparticles and trace elements in a pristine Norwegian fjord prospect for submarine tailings deposition. Statistical control of false-positive detections while minimizing the size detection limit was ensured using a novel raw signal processing. Scanning electron microscopy (SEM) and energy-dispersive X-ray spectroscopy (EDS) gave confirmative and qualitative information regarding particle morphology and composition. Following SP-ICP-MS screening for particles of 16 elements, particulate Al, Fe, Mn, Pb, Si and Ti were found and determined to mass concentrations in ng/L of 1–399, 1–412, below limit of detection (<LOD) - 269, <LOD - 1, <LOD - 1981 and <LOD - 127 ng/L with particle number concentrations up to 10^8 particles per liter. Total metals concentrations were at least an order of magnitude higher, at concentrations in μg/L of 1–12 for Al, 2–13 for Fe, 0.3–11 Mn, 0.02–0.5 for Pb, 46 to 318 Si and 0.04–0.4 for Ti. A strong depth dependence was observed for both trace elements and particles with concentrations increasing with depth. Our results provide a baseline for the fjord and new data on environmental levels of both total metals and metal containing nanoparticles including the vertical and horizontal distribution of natural nanoparticles.

1. Introduction

Nanoparticles (NPs) may be engineered, natural or incidental by-products of human activity. Whereas engineered NPs have received most attention, they are less abundant than incidental NPs, which in turn are outnumbered by natural NPs, whose role in biogeochemical processes remain poorly understood (Hochella et al., 2019). The ocean is the principal sink for NPs (Klaine et al., 2008). However, estimates of nanoparticle concentrations in the marine environment are either based on models backed by limited empiric evidence (Baker et al., 2014) or ensemble methods such as serial filtration or laser diffractometry. These methods are subject to various analytical artifacts and incapable of separating heteroaggregates with organic material from inorganic or metal particles. Quantitative studies using serial filtration cannot readily be compared due to variations in filter compositions, pore sizes and filter artifacts, and additionally give inadequate information regarding speciation or size distributions (Stumm and Morgan, 1996). This is evidenced by literature showing discrepancies that markedly exceed expected natural variations (Wilkinson and Lead, 2007), as well as recovery tests and comparison with size distributions obtained by electron microscopy (Stumm and Morgan, 1996).

Mechanistic models such as the Derjaguin–Landau–Verwey–Overbeek theory fail to predict NPs' extrinsic or media-dependent nature in complex environments and thus their stability in marine and natural waters (Rand and Ranville, 2019). As such, emphasis has been put on heuristic approaches to determining stability as both a function of dispersion characteristics (Klaine et al., 2008), including natural organic matter in controlled (Li et al., 2020) or natural

* Corresponding author. Institute of Marine Research, P.O. Box 1870 Nordnes, NO-5817, Bergen, Norway.
E-mail address: aresb@hi.no (A.S. Bruvold).

https://doi.org/10.1016/j.marenvres.2023.105975
Received 26 July 2022; Received in revised form 7 March 2023; Accepted 4 April 2023
Available online 11 April 2023

environments (Gondikas et al., 2020), and particle characteristics (Abdolahpur Monikh et al., 2018). Yet, empiric data regarding both dispersion and particle characteristics and composition in the environment are lacking due to the difficulty of analyzing environmentally relevant concentrations in complex matrices.

NPs have different bioavailability compared to bulk material or dissolved species causing concerns regarding the potential for bioaccumulation in the marine food chain (Mason, 2013). The lack of empirical data regarding NPs in the marine environment is further actualized by the continued increase in use of engineered nanoparticles as well as incidental sources including various industrial activities. Such activities include mineral mining performing submarine tailings deposition that may contain a large particle fraction in the sub-micrometer range, yet for which measurements are not straight-forward and therefore lacking (Farkas et al., 2021; Kvellestad, 2021). Lastly, nanoparticles are important biogeochemical components in the marine environment, whose concentration and speciation reflects e.g. chemical weathering environments and redox conditions (Hawkings et al., 2020).

Whereas detecting and quantifying NPs in environmentally relevant matrices remains a challenge, single particle inductively coupled plasma mass spectrometry (SP-ICP-MS) is an advancing technique allowing the detection of NPs at concentrations in the nanograms per liter range and below. Its potential as a screening technique for inorganic NPs in complex food matrices has previously been demonstrated (Vidmar et al., 2021). However, few validated methods for screening and quantification of NPs exist (Waegeneers et al., 2019). An additional source of uncertainty is the use of proprietary commercial algorithms for data processing based on non-discrete Gaussian statistics (Hendriks et al., 2019a; Laborda et al., 2020; Lockwood et al., 2021), often requiring the subjective manual adjustment of detection thresholds (see e.g. (Azimzada et al., 2021; Kinnunen et al., 2021; Rand et al., 2021; Vidmar et al., 2021)), or the potential acceptance of a large number of false positives. Analysis of seawater by SP-ICP-MS is challenging due to significant matrix effects and very low concentrations of NPs (Timerbaev et al., 2021). For this reason, off-line dilution to reduce matrix effects is unfeasible. Elevated background further complicates the discrimination of particle signals. A number of SP-ICP-MS studies perform spiking of engineered NPs in seawater (Timerbaev et al., 2021), but only three studies have used SP-ICP-MS for the determination of NPs containing Ti, Ce (Sanchís et al., 2020), Ti, Ce and Ag (Azimzada et al., 2021) and Ti and Pb (Gonzalez de Vega et al., 2022), using up to 50-fold dilution in deionized water or online aerosol dilution. These studies differed in terms of methodologies and metrics presented, but reported concentrations of Ti at 9 ng/L and 29 ng/L and from below the detection limit to $14 \bullet 10^9$ particles/L. Ce were detected in the 10^6s and 10^7s particles/L and Pb up to 10^7 particles/L.

The analytical requirements for trace metal sampling have been extensively studied and were largely established by the 1980s (LaFleur, 1976; Sturgeon et al., 1987). Most procedures practice chemical preservation by acidification using high-purity nitric or hydrochloric acid to prevent microbial activity, precipitation, surface adsorption and flocculation of metals (Sturgeon et al., 1987). However, this preservation has profound effects on speciation (Buffle and Leppard, 1995), which is of particular concern for NP detection and characterization due to their media-dependent properties, including dissolution. Strategies for sampling, sample preparation and sample introduction for NP determination are largely unstudied (Montaño et al., 2019).

While the body of knowledge on trace elements is vast in comparison to that on NPs, there is also missing knowledge on both concentration levels in various environmental compartments and their biogeochemical cycling. There is little data on trace elements in pristine coastal and fjord areas (Furness and Rainbow, 1990) as surveys are few and are generally only undertaken due to immediate concerns due to environmental discharges (Mason, 2013). However, expected concentrations and their variabilities are higher than in the open ocean (Mason, 2013) (Furness and Rainbow, 1990) (Elderfield, 2006). Reported concentrations are in the range of 0.1–6 μg/L for Mn and one to tens of μg/L for Fe (Mason, 2013). Other studies have reported temporal variations in the concentration of Al in fjord surface water, ranging from tens to hundreds of micrograms per liter (Simonsen et al., 2019), and vertical distributions of Fe and Al in the μg/L range increasing with depth in the Gullmarn fjord (Stolpe and Hassellöv, 2010).

The aim of this study was to develop and implement a multi-element screening method using SP-ICP-MS for the determination of nanoparticles in coastal seawater for the future surveillance of anthropogenic inorganic particles. We hypothesized that this method could detect differences in environmentally relevant concentrations between seawater sampled from six different depths at two locations corresponding to the outer and middle part of a relatively pristine fjord, Førde Fjord. Acidified and neutral samples were taken in parallel. Furthermore, the resulting survey data may serve for future comparison with locations subject to either more anthropogenic or natural input, such as nearby wastewater treatment plants, cities, submarine tailings deposition or glacial inputs. Specifically, the studied fjord is prospect for future submarine tailings deposition and the establishment of prior baseline data was thus of high relevance. As such, a traditional total metal determination was performed in parallel to NP determination. Scanning electron microscopy was performed as a confirmative method and to provide complementary qualitative information on particle compositions and morphology.

2. Materials and methods

2.1. Location

Førde Fjord (Fig. 1) is an approximately 40 km long fjord on the Norwegian west coast. The city of Førde with approximately 10 000 inhabitants is situated innermost of the fjord. It is a relatively pristine area, with a baseline study from 2017 indicating low concentrations of heavy metals and pollutants in indicator species (Kögel, 2019). Another baseline study from 2007 also indicates low concentrations of heavy metals yet elevated concentrations of titanium throughout the fjord (Brage Rygg, 2008). The fjord has a particularly rich fauna, also in comparison to other fjords in western Norway (Brage Rygg, 2008). Several rivers pour into the fjord, most notably Nausta and Jølstra. The Jølstra runs from Jølstravatnet and combines with the river Anga before reaching the fjord. Without Anga's input, Jølstra alone has a mean yearly discharge of approximately 50 m^3/s (Supplementary Table 1), receiving input from Europe's largest inland glacier, Jostedalsbreen. Nausta has a mean yearly discharge of approximately 20 m^3/s. The two sampling locations "inner" and "outer", shown in (Fig. 1), correspond to a location in the middle of the fjord and at the intersect of the fjord and the open ocean, respectively. The inner station is in proximity to planned submarine tailings deposition at up to 4 million metric tons per year. Modeling and in-situ measurements of currents indicates potential particulate transport both east and north in the (Staalstrøm and Molvær, 2009). The depth-dependent salinities were measured to 29–35‰ (Supplementary Fig. 1).

2.2. Sampling

Samples were acquired from RV Hans Brattstrøm on the 21st of October 2020, a day with minor precipitation and in a period of the year with relatively low discharge from the two major rivers. A 2.5 L Niskin plastic water sampler (Hydro-Bios, Altenholz, Germany) was used to collect all samples. The seawater samples were transferred to individual 120 mL and 250 mL polytetrafluoroethylene bottles (Nalgene FEP) using a standard oceanographic rosette (Hydro-Bios). Prior to sampling, the bottles and silicon tubings were acid washed in an acid steamer (Milestone traceCLEAN) using nitric acid (65% EMSURE for analysis, Merck) and rinsed five times using ultrapure water (UPW) (Merck Millipore). Corks were cleaned by an overnight acid bath of 10% vol:vol

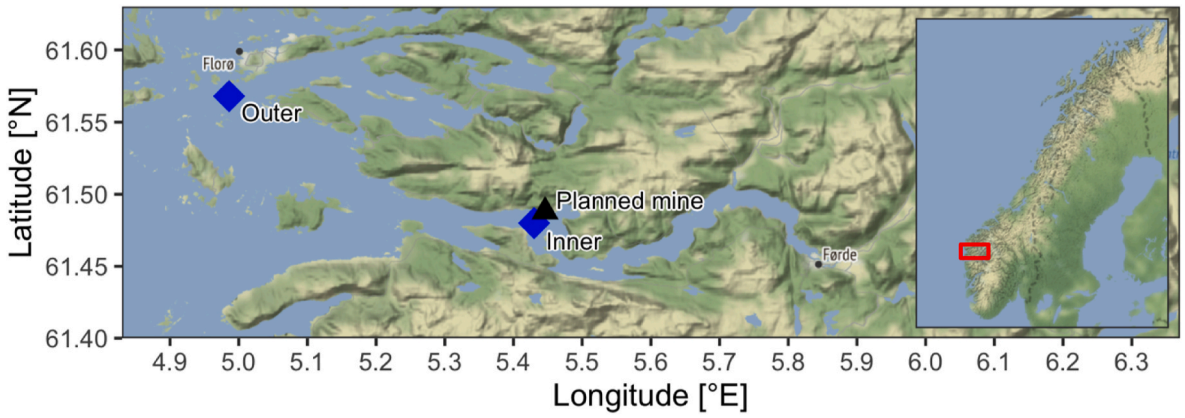

Fig. 1. Blue diamonds showing the location of the two stations at each of which samples at six depths were taken. The black triangle indicates the location for planned submarine tailings deposition. Map created by ggmaps using tiles from Stamen Design, under CC BY 3.0 and data by OpenStreetMap (Kahle and Wickham, 2013).

concentrated nitric acid inUPW. Niskin samplers were cleaned in two subsequent overnight acid baths of 10% vol:vol concentrated nitric acid and hydrochloric acid, respectively. Bottles and corks were dried overnight in a ventilated cupboard and wrapped in double plastic bags until and following sampling. Location inner was sampled at depths 325 (near bottom), 200, 100, 50, 20 and 10 m, whereas for location outer, samples were taken at depths 530 (near bottom), 200, 100, 50, 20 and 10 m. Sampling was performed in triplicate, one acidified for total metals, one acidified for NPs and one neutral for NPs. In the acidified sampling protocol for total metals and NPs, HCl (TraceMetal Grade, Fisher Chemical, Hampton, NH) was added to the sample using a pipette, corresponding to a final concentration of 0.5% vol:vol in the acidified sample. For the neutral sampling protocol, the sampled seawater was kept pristine. The samples were stored in the dark at approximately 4 °C.

2.3. Sample preparation

For SP-ICP-MS analysis, sub-sampling was done pipetting into 15 mL polypropylene tubes with a conical bottom (Cellstar, Greiner Bio-One, Kremsmünster, Austria) followed by shaking and vortex mixing for 10–15 s. The acidified sample set was sonicated using an ultrasonic bath for 20 min (Branson 8800 Series Ultrasonic Cleaner). No further sample preparation was performed prior to sample introduction. Six procedural blanks were made in the laboratory from UPW and added to an identical bottle as the seawater. UPW was produced using Elix Progard TNP and Milli-Q Advantage A10 (Merck Millipore, MA, USA) to a resistivity of 18.2 MΩ*cm. They were analyzed at different time intervals and used for determination of detection limits.

Preparation for total metals was performed pipetting into Teflon tubes pretreated by soaking in 0.7 M nitric acid for 24 h and rinsed in UPW. 1 mL of sample volume was added along with 1 mL HNO_3 and 8 mL of distilled, deionized water. Method blanks were prepared in parallel together with quality control samples of NASS-5, CASS-4 Seawater CRM for Trace Metals (National Research Council, Canada).

For the electron microscopy analysis, approximately 10 mL was pipetted out from the neutral sample. The sample was diluted with 50 mL UPW (Merck Millipore) and filtered through either 0.8 or 0.2 μm pore size polycarbonate (Isopore, Merck Millipore) filters placed on a sintered glass disc in a Büchner filtration apparatus. UPW was added again before a second filtration to ensure dispersion of particles on the filter. After drying, the filters were fixed on 25 mm aluminum SEM stubs covered with double-sided carbon adhesive disks (Agar Scientific, Essex, UK). Spots of carbon cement (Leit C, Agar Scientific) were added on the sides of the filters to improve conductivity between filter and aluminum stub. The filters were coated with a 10 nm platinum layer in a Cressington 208HR sputter coater (Cressington Scientific Instruments Ltd., Watford, United Kingdom) before SEM analysis.

2.4. Sample measurement

For SP-ICP-MS analysis, an Agilent 8900 Triple Quadrupole ICP-MS instrument (Agilent Technologies, Santa Clara, CA) with reaction and collision gas capability was used. It was equipped with a concentric MicroMist nebulizer in borosilicate glass and a Scott-type double pass spray chamber in quartz (temperature 2 °C). Online aerosol dilution, also known as high matrix introduction (HMI), was performed by an additional argon gas stream of 0.3 L/min between the spray chamber and torch, using a nebulizer gas flow of 0.7 L/min. Additional parameters for each measured isotope are given in Supplementary Table 2. H_2 reaction gas was used to mitigate spectral interference on Fe at m/z 56 and Si at m/z 28, whereas H_2 and O_2 and mass shift were used to reduce interferences on Ti at m/z 48 and TiO^+ at m/z 64. A calibration curve of minimum three points was established for each studied element using concentrations in the range of 0–200 μg/L, except for Ti, where a two-point calibration was used. Gold NP reference material (nanoComposix 60 nm NanoXact Gold Nanospheres Bare Citrate) was freshly prepared in UPW to a concentration of 500 ng/L and used to relate signal intensities to elemental mass and calculate transport efficiency and sample mass flow rate delivered to the detector as described elsewhere (Pace et al., 2011). Both NP and ionic gold were additionally spiked to seawater and acidified seawater matrices to assess matrix effects. Signal intensities for each element were recorded using a dwell time of 100 μs with acquisition time of 30 and 60 s for the pre-screening experiment and the final analysis, respectively. For the final analysis, each sample was measured three times (later referred to as measurements 1, 2 and 3) at 5 h intervals to assess repeatability. To avoid clogging and minimize memory effects, a rinsing procedure was performed after each sample: 5 s rinsing in UPW at 0.1 revolutions per second (RPS), followed by 15 s rinse in 1% v/v of each concentrated nitric acid (TraceSelect, Fluka Analytical, Switzerland), hydrochloric acid (TraceSelect, Fluka Analytical, Switzerland) and laboratory grade Triton™ X-100 (Sigma Aldrich) in UPW at 0.5 RPS, 30 s 5% HNO_3 at 0.5 RPS, and 60 s in UPW at 0.5 RPS.

For total metal analysis, a double focusing sector field inductively coupled plasma mass spectrometer, ELEMENT XR (Thermo Scientific, Bremen, Germany) was used with methane addition to the plasma in order to reduce polyatomic interferences and increase sensitivity (Rodushkin et al., 2005). It was equipped with a quartz torch with 1.5 inner diameter sapphire injector, nickel sampler cone, "X-type" skimmer cone, a two gas inlet port PFA spray chamber (Cetac Technologies, Omaha, NE, USA) micro-concentric MicroMist nebulizer, Fast SD2 auto-sampler (Elemental Scientific, Omaha, NB, USA). Internal

standard (indium of 2.5 μg/L) was employed for matrix effect correction. Additional parameters are supplied in Supplementary Table 3.

For SEM analysis, the filtered particles using the neutral protocol sampled at the outer station at a depth of 530 m were characterized by a SU6600 field emission scanning electron microscope (Hitachi, Tokyo, Japan) equipped with a Quantax 200 energy-dispersive X-ray (EDS) detector (Bruker Nano GmbH, Berlin, Germany). An accelerating voltage of 15 keV and a working distance (WD) of 10 mm were used during the analysis. Automated analysis of morphology and elemental composition of particles was performed using the feature module of the Esprit software (Bruker nano GmbH, Berlin, Germany). In the automatic particle analysis, high contrast backscatter (BSE) images were acquired for 100 fields in SEM at a magnification of 1300x for the 0.8 μm pore size filter and 2000x for the 0.2 μm pore size filter. The whole particle was scanned during X-ray acquisition. The elemental composition (atomic %) was quantified by the Esprit software using standardless peak-to-background ZAF correction. In addition, selected single particles were imaged and analyzed in SEM-EDS by spot analyses in secondary electron (SE) mode at 15 keV and 10 mm WD.

2.5. Data treatment and statistics

Data processing and statistical analysis were carried out in R version 4.1.0. All data and code are made available on Zenodo (Bruvold, 2023), GitHub or in the supplementary (Bruvold, 2022). The critical level for particle mass and number concentrations were set corresponding to a probability of <0.003 (α) of falsely rejecting the null hypothesis of no difference between a sample and six UPW blanks spaced evenly within the analytical batch and is in the following referred to as the limit of detection (LOD). For total metals, three times the standard deviation in blanks were used to calculate the LOD, considering the dilution factor. LODs were calculated using a Poisson confidence interval around the mean for number concentrations (Liddell, 1984), and from a mean plus three times the standard deviation for mass concentrations. Spectrograms were inspected individually, and a single spectrum was discarded as an outlier due to a highly fluctuating baseline that may be attributed to partial clogging: measurement two for iron at a depth of 10 m at the inner station. A new algorithm for automated raw signal processing based on particle discrimination by maximum peak intensity was developed and implemented to control the probability of false detections and reduce the number of undetected particle events. An unbiased background noise approximation was performed using a kernel density estimate and an intensity threshold derived under the assumption of Poisson distributed noise. This detection threshold was for each time scan set to a probability of 95% of observing at most one false positive per minute. For statistical analyses, for each element the response variable number of particles was modeled as a function of depth, station, sampling method and measurement time using a generalized linear model with a negative binomial error structure and log transformation, removing depths above 200 m. Significance of regression coefficients were determined using a Wald test without correcting for multiple comparisons. For the SEM-EDS analysis, contamination elements O, C, Pt, were removed and the atomic proportion rescaled to remaining elements. Mo, Ni, P, Pb, S, Zr were present at very low levels and were removed to avoid cluttering of compositional plots. For each particle, elements not quantifiable were also excluded from visualizations. Filtering on a particle basis was also done, removing particles in which $>50\%$ of the atomic proportion consisted of Na and Cl as these largely represented precipitates. Particles with circle equivalent diameter above 1.5 μm were removed to reduce the influence of aggregates. A single Ni and two Cr particles were also removed from the neutral samples, and two F-containing particles were removed from the acidified sample.

3. Results and discussion

3.1. Survey of inorganic nanoparticles and trace elements

A pre-screening was first performed on one sample set to determine which elements could be detected in particulate form. The lowest depth at the outer location had the highest metal concentration and was chosen for this purpose. The elements Al, Au, Ba, Cd, Ce, Co, Cr, Cu, Fe, Mn, Ni, Pb, Si, Ti, Zn and Zr were investigated due to being of relevance for environmental colloids, engineered NPs or mining waste. A decision criterion of 10 detected particle events per minute was selected, corresponding to approximately 4×10^6 particles per liter. The elements Al, Si, Ti, Mn, Fe and Pb met this threshold value and were chosen for further analyses. However, this does not exclude the possibility of other elements being present in samples that were not screened. While the standard sampling protocol with the introduction of acid into the seawater samples is a perturbation of their natural state, acidification is used for preservation for total metal analysis (Sturgeon et al., 1987). However, the change of dispersion characteristics is problematic for natural nanoparticles, for which e.g. dissolution or aggregation may occur as the present findings illustrate. Using acidified and neutral sampling in parallel, complementary information on the particle speciation can be obtained.

Results from the total metal analysis of elements of Al, Fe, Mn, Pb, Si and Ti are shown in Fig. 2. Nutrient-type vertical distributions with increasing concentrations with increasing depth are largely observed (Libes, 2009). Magnitudes are similar for both stations, the inner station exhibiting more variability consistent with a fjord environment. The strong depth dependence on the vertical profiles of Fe, Mn, Al and Si implies resuspension and redox-mediated release from sediments to the overlying water to be the dominating source for these elements (Stumm and Morgan, 1996). The surface enrichment observed for e.g. Al suggests additional atmospheric or riverine input, which would be expected to be affected by the period of low precipitation. Lead is an exception to mentioned trends, exhibiting a mid-to-high-depth maxima consistent with an atmospheric anthropogenic input characteristic for lead (Stumm and Morgan, 1996). Similar depth dependence and large seasonal variations were also observed in the Gullmarn fjord for Fe and Al, with concentrations from micrograms to tens of micrograms per liter (Stolpe and Hassellöv, 2010), otherwise corroborating with levels determined in coastal and fjord waters for the respective elements (Mason, 2013; Simonsen et al., 2019; Botté et al., 2022).

Total metals have predictive value for the particulate mass concentrations yet exhibits more variability with depth. The particulate elemental fractions in the detectable range were in all cases below 5% and with concentrations increasing with depth (Fig. 3). Concentrations for particulate Al were in the range 1 ng/L to 399, Fe 1–412 ng/L, Mn LOD – 269 ng/L, Pb LOD – 1 ng/L, Si LOD - 1981 ng/L and Ti LOD -127 ng/L in the detectable range (Supplementary Table 4). This data is comparable to the recent report of particulate Ti at approximately 9 ng/L and 29 ng/L in surface seawater near Vancouver and Casablanca, respectively (Azimzada et al., 2021). Literature from traditional colloid measurements using ultrafiltration also report higher concentrations of particulate Fe and Mn near the bottom, whereas Al and Si may also be present higher in the water column (Skei and Melsom, 1982). Higher concentrations of Al and Si in fjord surface water are typically correlated with river water flux, whereas Si may additionally be of biogenic origin (Skei and Melsom, 1982). The low concentrations of Al and Si in the surface water is consistent with the low river flux and biological activity at the time of sampling. There is ambiguity in terms of the observed particulate versus dissolved fraction for a number of elements. Geochemistry predict manganese to be present as particulate manganese oxide species (Langen et al., 1997), yet measurements using filtration often report manganese primarily in the dissolved fraction (Wells, 2002), as was also found in the present study. Iron is predominantly present in the colloidal phase (Barnard and Guo, 2012) (Wells, 2002),

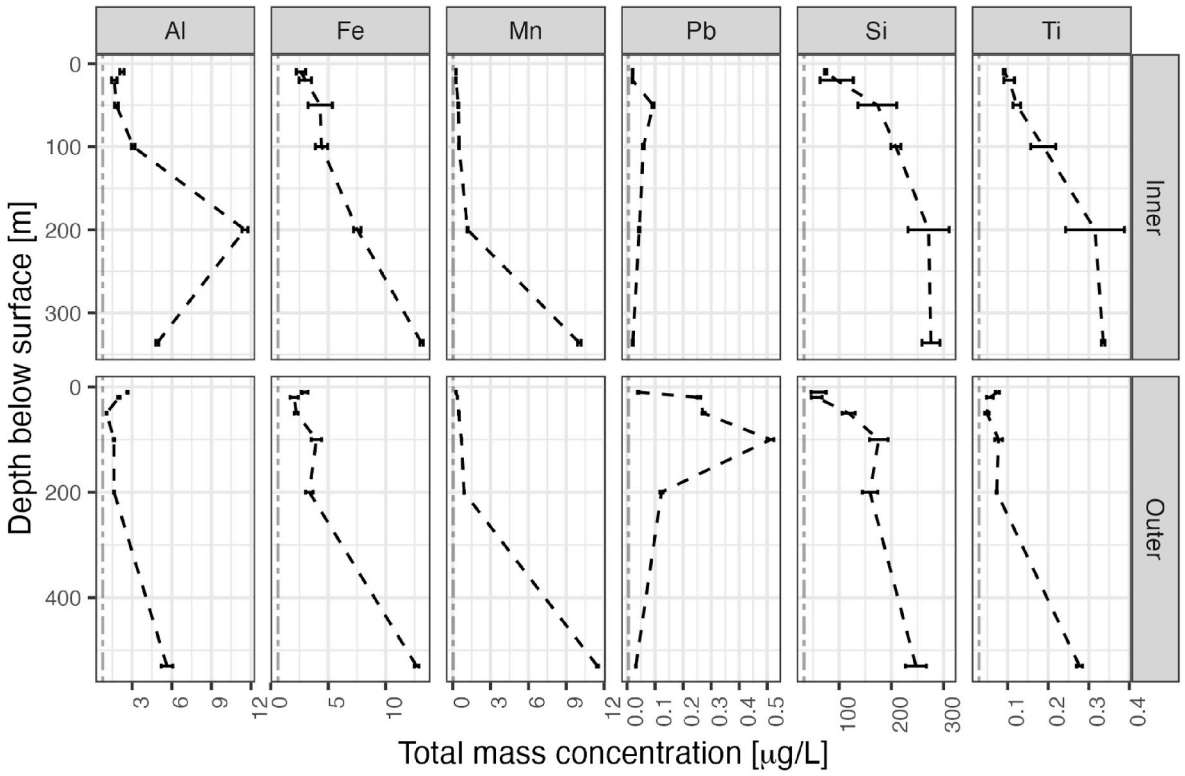

Fig. 2. Total metal concentrations in dependence of depth below water surface for the two sampling locations as determined by the sector field ICP-MS. Error bars indicates standard error of the mean of two analytical replicates. Vertical line denotes the LOD.

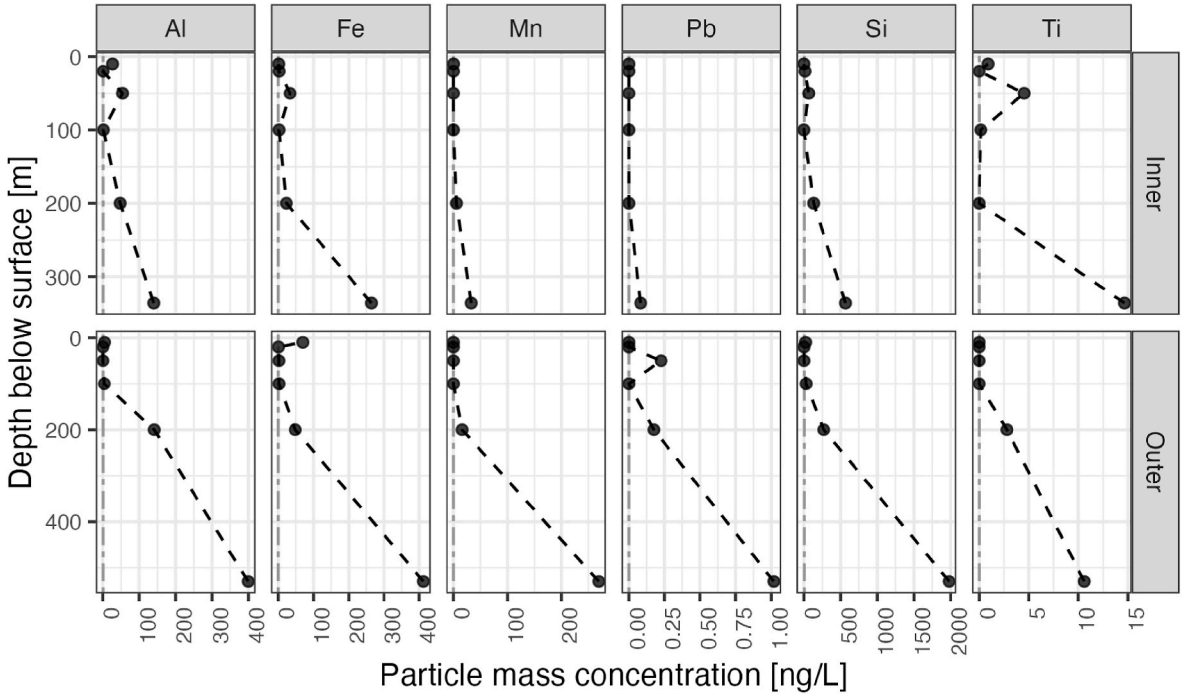

Fig. 3. Particulate mass concentrations plotted against depth for the neutral samples as determined by SP-ICP-MS. The detection limit is indicated by the vertical line.

including adsorbed to organic material, and as iron oxides in or near the nano-range (Wells and Goldberg, 1992). The present work suggests that the inorganic colloidal or nanoparticulate fraction represents a relatively minor fraction of the total metal, although underestimation is probable due to settling or transformation during analysis and storage, size-bias and upper detection limit of the sample introduction system and the ICP-MS. While seldom practical, ideally analysis should be carried out in-situ or within hours or days after sampling. The use of antimicrobial agents or anticoagulants is also possible, however, the influence of these have not been explored (Buffle and Leppard, 1995). As

the mass per particle is a cubic function of its diameter, the upper detection limit of the technique is consequential for mass concentrations and should be accurately established for SP-ICP-MS. Alternatively, additional size fractionation could be performed using centrifugation, sedimentation, filters or field flow fractionation, yet at the cost of decreased sample throughput and potentially introducing new analytical artifacts.

Number concentrations of detected particulate species of each element are available in the supplementary material (Supplementary Fig. 4). A strong depth dependence was observed with generally higher concentrations at the outer station ($p < 0.001$), which may be attributed to multiple physical and chemical parameters including dynamics of the water bodies, sediment composition or redox composition (Mason, 2013). Number concentrations were in all cases below 10^8 particles per liter. This is lower than two other reports of Ti and Ce concentrations from below LOD to 10^8 (Sanchís et al., 2020), and Ti and Ce in the 10^8s and 10^6 s s to 10^7s, respectively (Azimzada et al., 2021). A recent study reported Pb at concentrations of approximately 10^7 particles per liter and above 10^{10} for Ti in Port Philip Bay, Melbourne, Australia (Gonzalez de Vega et al., 2022). However, results are not directly comparable due to areas being subject to more anthropogenic impact and being sampled from surface water. The sample treatment differed both with respect to the use of filters, sonication and dilutions.

Moreover, the limits of detection will be conflicting due to both different sensitivities and statistical assumptions. In many cases a x sigma threshold more appropriate for millisecond dwell time data is utilized. Whereas Chebyshev's inequality guarantees 0.3% to be within an interval of ± three standard deviations from the mean given a Gaussian distributed background, it reduces to around 11% in the most general case (Guthrie, 2020). A simulation study is included to demonstrate a worst-case scenario for the number of false positives because of the inappropriate assumption of Gaussian distributed noise (Supplementary Fig. 5). Detection thresholds should be established on the basis of the actual background discrete noise distribution, which is more appropriately modeled by Poisson statistics as discussed elsewhere (Hendriks et al., 2019a; Laborda et al., 2020; Lockwood et al., 2021). The upper limit of detection has not been fully established for SP-ICP-MS with reports ranging from several μm (Meermann and Nischwitz, 2018) to 8 μm (Taylor, 2001). Signal per mass is non-linear for larger particles (Olesik and Gray, 2012), transmission efficiency decreasing with increasing size (Kammer et al., 2012). The upper size detection limit would be expected to be dependent on instrumental parameters, setup, matrix and analyte, and have been reported to be above 1 μm for SiO_2 (Kammer et al., 2012). It is not fully explored how aggregation affects sample introduction and vice versa, yet it is known that smaller aggregates can be measured and used to study aggregation kinetics (Donahue et al., 2020) (Rand, 2019). Though, it is not clear to what extent larger aggregates may be sheared apart or selectively removed due to their bulkiness and mass (Rand, 2019). Suppression or enhancement may also arise due to the presence of other elements in multielement particles.

Particle masses spanned several orders of magnitude and were generally most frequent around 1 fg, the smallest detected particles for each element of similar orders of magnitude except for Si due to reduced sensitivity caused by the presence of dissolved background and interferents (Fig. 4). Median spherical equivalent diameters were 232, 103, 104, 53, 379 and 155 nm for Al, Fe, Mn, Pb, Si and Ti, respectively. These were based on assumptions of orthoclase feldspar, goethite, birnessite, which are dominant minerals for Al, Si, Fe and Mn (Barrón and Torrent, 2013), whereas anglesite and titanite were assumed for Pb and Ti. Compositional information is included in **(Supplementary Table 5)**. Nevertheless, the diameter is proportional to the cubic root of the elemental density and will for this reason give meaningful estimates despite inaccurate assumptions.

3.2. *Technical and methodological considerations for single particle analysis*

In the present work, undiluted seawater was introduced to the instrument, performing online aerosol dilution by an additional argon gas flow between spray chamber and torch. Further, collision/reaction cell technology was used for some of the studied isotopes to overcome spectral interference. Thus, it was of interest to investigate the influence of the seawater matrix and the dilution gas on ionic and NP signal. Due to the lack of well-characterized NPs of other relevant compositions, the influence of these parameters was studied for Au NPs (60 nm) and ionic standards. Unless corrected for, these parameters may result in over- or underestimation of mass concentrations and sizes, and may explain size differences reported between seawater and river-, lake- and rainwater (Azimzada et al., 2021). To investigate repeatability, three replicate measurements of the samples were performed.

Relative to UPW, up to 52% and 63% reduction in mean signal intensity was observed for ionic Au in neutral and acidified seawater, respectively. For Au NP signals, as represented by the integrated peak areas, a similar signal suppression of 47% and 49% for neutral and

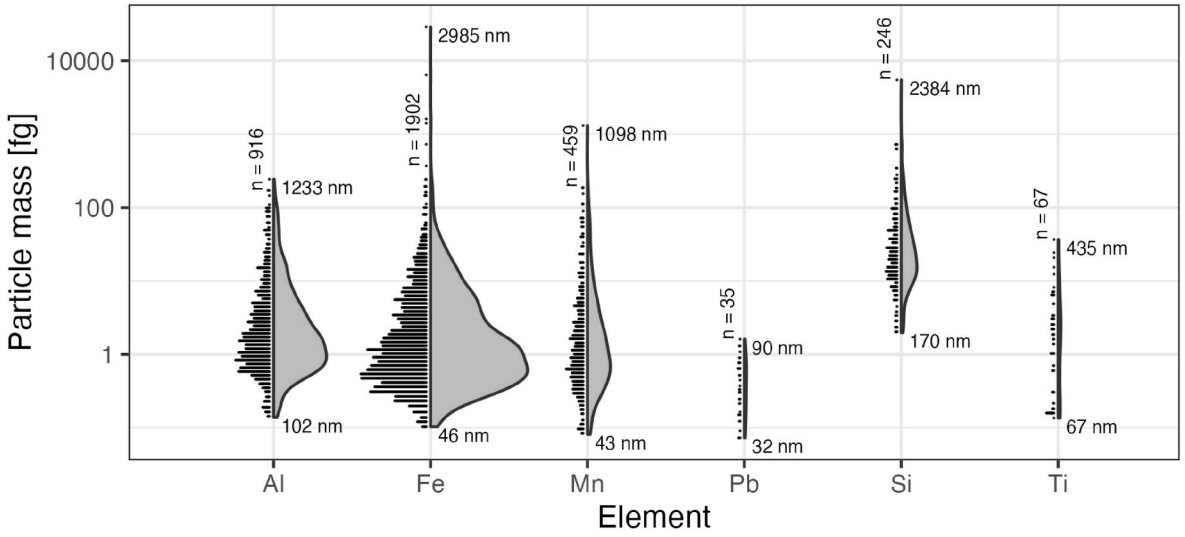

Fig. 4. Mass distributions in femtograms for each element across all depths and both stations as determined with SP-ICP-MS using the neutral sampling protocol. Histogram bins are evenly spaced in the log space with kernel density estimate to the right. Specified are number of detected particles as well as maximum and minimum diameters.

acidified seawater was observed (Supplementary Fig. 2). Aerosol dilution was associated with an additional similar decrease in mean peak intensity for Au NPs in UPW when compared to not using aerosol dilution. Lastly, a downward signal trend of around 30% was observed over the experimental run of approximately 20 h when performing repeated measurement of ionic standards, which is likely due to instrumental drift and gradual deposition on to the cones not removed efficiently by rinsing protocols and blanks (Agatemor, 2011). To correct for the signal suppression by the seawater matrix, a pragmatic approach was chosen: Au NPs were prepared in both, UPW and seawater. Ionic standards of all studied elements were prepared in UPW (i.e. not "matrix-matched") due to the risk of metal surface adsorption or precipitation in seawater. A correction factor of 0.515 corresponding to the mean peak area ratio between Au NP spiked to seawater and UPW matrices was determined and then used for correcting the response factors of all other elements. Ideally, the correction factor should have been determined for NPs of each studied element. However, suitable NPs of respective composition were not available.

Matrix effects from seawater have been extensively studied using traditional ICP-MS, in which up to 67% reduction has been reported attributed to reduced ionization, space charge effects of ion lenses and collisional scattering (Agatemor, 2011) (Taylor, 2001). For single particle ICP-MS, a single work reports the suppression of the NP signal in (diluted) seawater (Toncelli et al., 2016). More generally, one (not peer reviewed) study reported lower suppression of particulate Au than ionic Au species (Montaño et al., 2016), whereas Kinnunen reported suppression only for the particulate form in a trisodium acetate matrix for Au (Kinnunen et al., 2021). A systematic study using microdroplets has previously shown that NP Au and microdroplet Au exhibited similar yet slightly different matrix effects in HNO_3 and HCl (Hendriks et al., 2019b), and others have reported different suppression between ionic and particulate species (Liu et al., 2017; Vidmar et al., 2018). For ions it is difficult to distinguish changes in the transport efficiency at the sample introduction stage from what is occurring further within the plasma, interface, ion optics, MS system and detector. As opposed to ionic species, a particle is either introduced to the plasma or not. As such, suppression of NP peak area signals in a matrix can give insights into the isolated matrix effects occurring after the introduction system. This justifies the approach of determining transport efficiency in UPW and correcting for any matrix induced suppression based on analyte particle signals. While interlaboratory comparisons show agreement in terms of determined particle sizes in complex matrices between different laboratories and instruments (Geiss et al., 2021), further studies should be performed using well-characterized monodisperse reference materials and open-source signal processing to identify the specific driving variables for the observed effects and how to appropriately correct for various potential sources of error due to different particle elemental compositions, densities, sizes/masses and ionization efficiencies in order to ascertain the trueness of the technique.

While aerosol dilution was used to retain dispersion characteristics by avoiding off-line aqueous dilution of the samples, reduce potential contamination and to increased practicality, it may result in reduced instrumental sensitivity and thus an increase in size detection limit. A previous study hypothesizes the sensitivity decrease to be caused by an off-axis flow path of the particles as a result in changes of the optimal flow, plasma temperature and residence time (Kálomista et al., 2017). Nonetheless, this effect would not cause a bias as calibrations and measurements were performed using identical parameters.

As shown in Supplementary Fig. 14, a time dependency of measured particle number concentrations was observed. A post hoc analysis substantiated this for Si, Al, Fe and Ti ($p < 0.01$), whereas no such dependency could be inferred for Pb ($p = 0.67$) and Mn ($p = 0.91$). Surface adsorption, aggregation and sedimentation at room temperature are competing mechanisms that may cause the time dependency observed for the measurements. The positioning of the autosampler probe was near the bottom of the sample tubes throughout the sequence and thus equal for all samples. Controlling the vertical placement could allow using this information and Stoke's law to investigate the relative importance of these effects.

3.3. Scanning electron microscopy with energy dispersive x-ray spectroscopy

Elemental analysis complemented with cluster analysis of individual particles showed major crustal elements Si, Al, Fe, Mn and Ca to be dominant (Fig. 5). Many particles appeared to be of biotic origin including coccoliths of Emiliania Huxleyi (P. Westbroek et al., 1984) and what resembles appendages of iron and manganese sequestering bacteria (Heldal et al., 1996) (Fig. 5F). Other particles were natural NPs or colloids consistent with e.g. alkali feldspars (Fig. 5C), silicates **(B)**, iron oxides **(E)**, manganese-iron oxides **(A)** and calcium carbonates **(D)** (EDS spectra in Supplementary Figs. 6–11). The morphology of most iron, manganese and manganese-iron oxides resembled the bacterial appendages and may have the same source. Aluminum silicates generally had a smooth morphology and were likely of abiotic origin as is generally the case with Al-based particles (Ohnemus et al., 2019), as did silicon-based particles. Some morphologically and compositionally distinctive particles of e.g. iron oxides and dolomite were also found. Quantitative SEM-EDS corroborated with SP-ICP-MS underlining the presence of major crustal elements Si, Al, Fe and Mn. Ti was not detected, but was measured only in the ng/L range (Fig. 3). SEM additionally detected Ca, Cl, K, Mg and Na, which were not screened for using SP-ICP-MS. Na and Cl were commonly present both as salt particles and a constituent due to their abundance in seawater causing crystallization. Compositional data for the major elements of each particle revealed a strong correlation between Si and Al: Si for every particle analyzed making up a greater atomic proportion than Al (Supplementary Fig. 16). Thus, aluminum particles were in all likelihood aluminum silicates, and not aluminum oxides such as gibbsite, which is another dominant particulate aluminum form (Botté et al., 2022). In the acidified samples, only Si and Si–Al-particles were detected, signifying a pH-dependent dissolution of Fe, Mn and Pb-based particles and aggregates (Supplementary Fig. 13). This further indicates that no single particle phases contained both Si/Al in combination with Fe/Mn, as otherwise particulate Fe and Mn would be detected also in the acidified samples. Mn primarily cooccurred with Fe, whereas Fe was associated with all elements. Fe, Mn and Si were all present as the major atomic constituent of a particle (Supplementary Fig. 12), e.g. in iron oxides, manganese oxides, quartz and aluminum silicates as displayed in (Fig. 5). Al was primarily a minor constituent within a relatively narrow range of atomic proportions and K was often found alongside Al and Si. However, particles were in general highly heterogenous in composition making exact mineral classifications based on relative atomic proportions impractical as the in-cluster variation illustrates (Fig. 5). Natural nanoparticles are complex, often exhibiting coatings, mixed phases, aggregation, adsorbed ions and precipitates (von der Heyden et al., 2014; Montaño et al., 2022). Direct comparisons of size distributions between the two methods were generally unsubstantiated due to the different elements being represented by multiple complex particle populations with widely varying elemental compositions. Moreover, SEM determines the optically projected area's circle equivalent diameter, whereas SP-ICP-MS determines the mass equivalent spherical diameter. For the seemingly homogenous Al-particle population, a comparison between size distributions showed a more polydisperse distribution and larger sizes for SEM (Supplementary Fig. 15). However, aluminum silicates are typically sheet-like (Wilkinson and Lead, 2007), and will preferentially deposit projecting the greatest external dimensions. For electron microscopy, filtration- and drying artifacts such as the selective retention of larger particles, precipitation of salts and aggregation as well as biases due to the image recognition software may also cause a substantial overestimation of particle sizes. Natural nanoparticles have been hypothesized to exhibit log-normal distribution

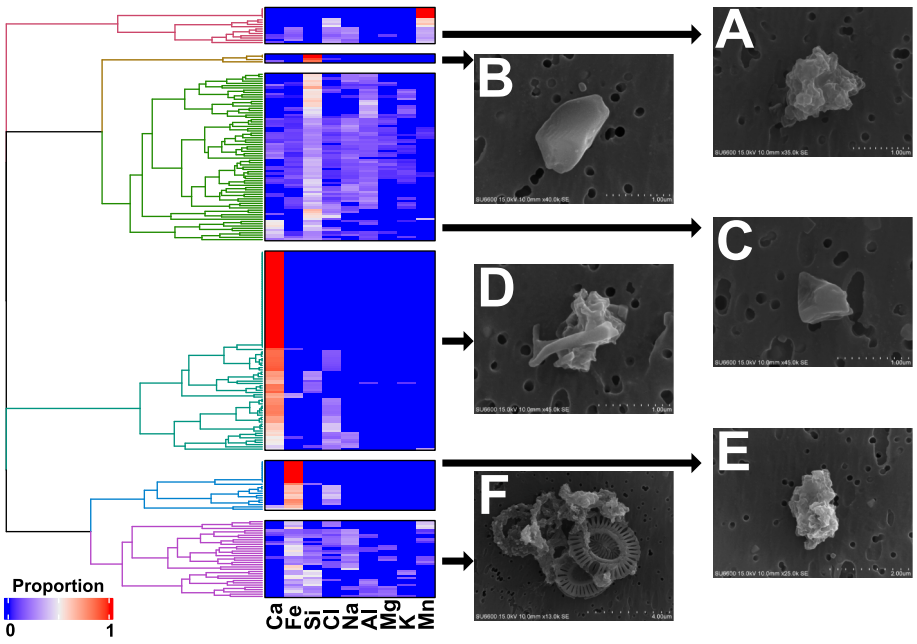

Fig. 5. Hierarchical agglomerative clustering on the cleaned EDS data from the neutral sample using complete linkage (Gu, 2022). SEM micrographs displays (A) manganese-oxide, (B) silicate, (C) aluminum silicate (K–Al–Si, (D) iron oxide-calcium heteroaggregate), (E) iron oxide, (F) Fe, Mn–Fe and Ca-aggregate).

(Wilkinson and Lead, 2007). Our data showed a polydisperse size distribution, equivalent diameters ranging from approximately 300 nm to 11 μm as determined by SEM (Supplementary Fig. 12). The employed sample preparation including filtration will result in an underestimation of smaller particles. However, if abundant, some retention of smaller particles would also be expected (Jreije et al., 2022). The results are comparable to reports with mean sizes around 700 nm for iron colloids (von der Heyden et al., 2014). Although differing detection limits, relative abundance on a particle number basis was in reasonable agreement between the two techniques employed. The present findings corroborate with natural NPs previously characterized in coastal surface seawater in terms of particle compositions (Wells and Goldberg, 1992), but did not detect particles below 100 nm. The two techniques are highly complementary, SP-ICP-MS as a robust and precise platform providing quantitative data suitable for statistical inference yet relies on correct compositional and morphological assumptions for accurate size determination. SEM-EDS provides accurate qualitative data on particle composition and morphology, which of special relevance for complex multi-element natural particles.

4. Conclusion

A platform for precisely determining mass and number concentrations of inorganic NPs in seawater using SP-ICP-MS was developed and implemented in combination with quantitative SEM-EDS analysis. As hypothesized, this method detected trends vertically and horizontally and served to provide new data on the distributions of inorganic nanoparticles in seawater. A screening for NPs of 16 elements in one sample using SP-ICP-MS found Al-, Fe-, Mn-, Pb-, Si- and Ti-based particles to be dominant. A subsequent survey of both total metals and NPs of these elements showed that the inorganic particles represented a relatively minor fraction at no more than a few percent of the total metals, at concentrations mostly in the hundreds of ng/L. A strong depth dependence was found for both forms. The two stations showed comparable levels of total metals, but lower NP concentrations and a weaker correlation between particulate and total concentrations in the inner fjord. Quantitative SEM-EDS screening displayed credible agreement in terms of both elements detected and their relative abundance, yet overestimated sizes in comparison to SP-ICP-MS. No particles below 250 nm were found using SEM-EDS, although the filtration for sample preparation would underestimate this fraction. The most dominant particulate forms were identified using secondary electron imaging complemented with cluster analysis of quantitative SEM-EDS data and recognized to be aluminum silicates, calcium-based particles, iron oxides and manganese oxides. These were often complex in composition and morphology, showing non-spherical geometries and rough surface textures, heteroaggregation, coatings or adsorbed precipitates. The present work demonstrates a sensitive and precise platform suitable for the determination of inorganic NPs in the marine environment and provides quantitative survey data of metals and inorganic particles. With increasing sensitivities and emerging potential for simultaneous multi-element characterization using time-of-flight detectors, new insights into particle occurrence and dynamics can be gained. This holds relevance both for the surveillance of anthropogenic activities including submarine tailings deposition and the advancement of our understanding of natural geochemical processes in the principal yet underexplored compartment that is the marine environment.

Author statement

ASB: Conceptualization, methodology, software, formal analysis, investigation, data curation, writing – original draft, visualization. AMB: Methodology, writing – review & editing, validation. TK: Investigation (SEM), writing – original draft (SEM) and editing, methodology. KL: Methodology, writing – review & editing, supervision, funding acquisition. SV: Methodology, writing – review & editing, supervision, funding acquisition.

Funding sources

The work was primarily funded through the Institute of Marine Research project Marine nanoparticles (15318). The cruise was funded through the Coast-risk project under the Norwegian Research Council (project 299554) and Institute of Marine Research project 15507–02.

Declaration of competing interest

The authors declare that they have no known competing financial

interests or personal relationships that could have appeared to influence the work reported in this paper.

Data availability

Raw data, code and statistical anlyses are made available through Zenodo and GitHub.

Acknowledgments

We kindly thank Ingrid Johnsen for organizing the cruise, Michael S. Bank for sampling the water, the engineers at IMR's inorganic lab for setup, assistance and maintenance of the ICP-MS instrumentation and Monica Sanden for support and supervision regarding biological and non-scientific aspects. The R-club of The University of Bergen is also thanked for providing an inclusive environment for coding input and advice. Janja Vidmar is thanked for an introduction to practical and theoretical aspects of single particle instrumentation.

Appendix A. Supplementary data

Supplementary data to this article can be found online at https://doi.org/10.1016/j.marenvres.2023.105975.

References

Abdolahpur Monikh, F., Praetorius, A., Schmid, A., Kozin, P., Meisterjahn, B., Makarova, E., et al., 2018. Scientific rationale for the development of an OECD test guideline on engineered nanomaterial stability. NanoImpact 11. https://doi.org/10.1016/j.impact.2018.01.003.

Agatemor, C., 2011. Matrix effects in inductively coupled plasma mass spectrometry: a review. Anal. Chim. Acta 18. https://doi.org/10.1016/j.aca.2011.08.027.

Azimzada, A., Jreije, I., Hadioui, M., Shaw, P., Farner, J.M., Wilkinson, K.J., 2021. Quantification and characterization of Ti-, Ce-, and Ag-nanoparticles in Global surface waters and precipitation. Environ. Sci. Technol. 55, 9836–9844. https://doi.org/10.1021/acs.est.1c00488.

Baker, T.J., Tyler, C.R., Galloway, T.S., 2014. Impacts of metal and metal oxide nanoparticles on marine organisms. Environ. Pollut. 186, 257–271. https://doi.org/10.1016/j.envpol.2013.11.014.

Barnard, A.S., Guo, H. (Eds.), 2012. Nature's Nanostructures. Pan Stanford Publications, Singapore.

Barrón, V., Torrent, J., 2013. Iron, manganese and aluminium oxides and oxyhydroxides. Eur. Mineral Union Notes Mineral 14, 297–336. https://doi.org/10.1180/emu-notes.14.9.

Botté, A., Zaidi, M., Guery, J., Fichet, D., Leignel, V., 2022. Aluminium in aquatic environments: abundance and ecotoxicological impacts. Aquat. Ecol. https://doi.org/10.1007/s10452-021-09936-4.

Bruvold, Are Sæle, 2022. GitHub Repository for Distribution of Inorganic Nanoparticles and Trace Elements in a Norwegian Fjord (Available at: github.com/arebruvold/fordefjorden_distribution).

Buffle, J., Leppard, G.G., 1995. Characterization of aquatic colloids and macromolecules. 2. Key role of physical structures on analytical results. Environ. Sci. Technol. 29, 2176–2184. https://doi.org/10.1021/es00009a005.

Donahue, N.D., Francek, E.R., Kiyotake, E., Thomas, E.E., Yang, W., Wang, L., et al., 2020. Assessing nanoparticle colloidal stability with single-particle inductively coupled plasma mass spectrometry (SP-ICP-MS). Anal. Bioanal. Chem. 412, 5205–5216. https://doi.org/10.1007/s00216-020-02783-6.

Elderfield, H., 2006. In: Elderfield, H. (Ed.), Treatise on Geochemistry. 6: the Oceans and Marine Geochemistry/Vol. Elsevier, Amsterdam Heidelberg, p. 1.

Farkas, J., Nordtug, T., Svendheim, L.H., Amico, E.D., Davies, E.J., Ciesielski, T., et al., 2021. Effects of mine tailing exposure on early life stages of cod (Gadus morhua) and haddock (Melanogrammus aeglefinus). Environ. Res. 200, 111447 https://doi.org/10.1016/j.envres.2021.111447.

Furness, R.W., Rainbow, P.S. (Eds.), 1990. Heavy Metals in the Marine Environment. CRC Press, Boca Raton, Fla.

Geiss, O., Bianchi, I., Senaldi, C., Bucher, G., Verleysen, E., Waegeneers, N., et al., 2021. Particle size analysis of pristine food-grade titanium dioxide and E 171 in confectionery products: interlaboratory testing of a single-particle inductively coupled plasma mass spectrometry screening method and confirmation with transmission electron microscopy. Food Control 120, 107550. https://doi.org/10.1016/j.foodcont.2020.107550.

Gondikas, A., Gallego Urrea, J., Halbach, M., Derrien, N., Hassellöv, M., 2020. Nanomaterial fate in seawater: a rapid sink or intermittent stabilization? Front. Environ. Sci. 8 https://doi.org/10.3389/fenvs.2020.00151.

Gonzalez de Vega, R., Lockwood, T.E., Xu, X., Gonzalez de Vega, C., Scholz, J., Horstmann, M., et al., 2022. Analysis of Ti- and Pb-based particles in the aqueous environment of Melbourne (Australia) via single particle ICP-MS. Anal. Bioanal. Chem. 414, 5671–5681. https://doi.org/10.1007/s00216-022-04052-0.

Gu, Z., 2022. Complex heatmap visualization. iMeta 1. https://doi.org/10.1002/imt2.43.

Guthrie, W.F., 2020. NIST/SEMATECH E-Handbook of Statistical Methods (NIST Handbook 151). https://doi.org/10.18434/M32189.

Hawkings, J.R., Skidmore, M.L., Wadham, J.L., Priscu, J.C., Morton, P.L., Hatton, J.E., et al., 2020. Enhanced trace element mobilization by Earth's ice sheets. Proc. Natl. Acad. Sci. U.S.A. 117, 31648–31659. https://doi.org/10.1073/pnas.2014378117.

Heldal, M., Fagerbakke, K., Tuomi, P., Bratbak, G., 1996. Abundant populations of iron and manganese sequestering bacteria in coastal water. Aquat. Microb. Ecol. 11, 127–133. https://doi.org/10.3354/ame011127.

Hendriks, L., Gundlach-Graham, A., Günther, D., 2019a. Performance of sp-ICP-TOFMS with signal distributions fitted to a compound Poisson model. J. Anal. Atomic Spectrom. 34, 1900–1909. https://doi.org/10.1039/c9ja00186g.

Hendriks, L., Ramkorun-Schmidt, B., Gundlach-Graham, A., Koch, J., Grass, R.N., Jakubowski, N., et al., 2019b. Single-particle ICP-MS with online microdroplet calibration: toward matrix independent nanoparticle sizing. J. Anal. Atomic Spectrom. 34, 716–728. https://doi.org/10.1039/c8ja00397a.

Hochella, M.F., Mogk, D.W., Ranville, J., Allen, I.C., Luther, G.W., Marr, L.C., et al., 2019. Natural, incidental, and engineered nanomaterials and their impacts on the Earth system. Science 363, eaau8299. https://doi.org/10.1126/science.aau8299.

Jreije, I., Hadioui, M., Wilkinson, K.J., 2022. Sample preparation for the analysis of nanoparticles in natural waters by single particle ICP-MS. Talanta 238, 123060. https://doi.org/10.1016/j.talanta.2021.123060.

Kahle, D., Wickham, H., 2013. ggmap: spatial visualization with ggplot2. R J. 5, 144. https://doi.org/10.32614/RJ-2013-014.

Kálomista, I., Kéri, A., Galbács, G., 2017. Optimization of plasma sampling depth and aerosol gas flow rates for single particle inductively coupled plasma mass spectrometry analysis. Talanta 172, 147–154. https://doi.org/10.1016/j.talanta.2017.05.051.

Kammer, F. von der, Ferguson, P.L., Holden, P.A., Masion, A., Rogers, K.R., Klaine, S.J., et al., 2012. Analysis of engineered nanomaterials in complex matrices (environment and biota): general considerations and conceptual case studies. Environ. Toxicol. Chem. 31, 32–49. https://doi.org/10.1002/etc.723.

Kinnunen, V., Perämäki, S., Matilainen, R., 2021. Optimization of instrumental parameters for improving sensitivity of single particle inductively-coupled plasma mass spectrometry analysis of gold. Spectrochim. Acta B Atom Spectrosc. 177, 106104 https://doi.org/10.1016/j.sab.2021.106104.

Klaine, S.J., Alvarez, P.J.J., Batley, G.E., Fernandes, T.F., Handy, R.D., Lyon, D.Y., et al., 2008. Nanomaterials in the environment: behavior, fate, bioavailability, and effects. Environ. Toxicol. Chem. 27, 1825–1851. https://doi.org/10.1897/08-090.1.

Kögel, T., 2019. Analysis of Heavy Metals, Other Elements and Persistent Organic Pollutants in Seafood from the Førdefjord 2017. Institute of Marine Research.

Kvellestad, Agnar, 2021. A Permitted Discharge of Mining Waste to the Marine Environment - Critical Review Regarding Heavy Metals and Chemicals. Norwegian University of Life Sciences.

Laborda, F., Gimenez-Ingalaturre, A.C., Bolea, E., Castillo, J.R., 2020. About detectability and limits of detection in single particle inductively coupled plasma mass spectrometry. Spectrochim. Acta B Atom Spectrosc. 169, 105883 https://doi.org/10.1016/j.sab.2020.105883.

LaFleur, P.D., 1976. Accuracy in trace analysis : sampling. sample handling, analysis I, 684.

Langen, P.J.V., Johnson, K., Coale, K., Elrod, V., 1997. Oxidation kinetics of manganese (II) in seawater at nanomolar concentrations. Geochem. Cosmochim. Acta 10.

Li, Z., Shakiba, S., Deng, N., Chen, J., Louie, S.M., Hu, Y., 2020. Natural organic matter (NOM) imparts molecular-weight-dependent steric stabilization or electrostatic destabilization to ferrihydrite nanoparticles. Environ. Sci. Technol. 54, 6761–6770. https://doi.org/10.1021/acs.est.0c01189.

Libes, S.M., 2009. Introduction to Marine Biogeochemistry, second ed. Academic Press, Amsterdam ; Boston.

Liddell, F.D., 1984. Simple exact analysis of the standardised mortality ratio. J. Epidemiol. Community Health 38, 85–88. https://doi.org/10.1136/jech.38.1.85.

Liu, J., Murphy, K.E., Winchester, M.R., Hackley, V.A., 2017. Overcoming challenges in single particle inductively coupled plasma mass spectrometry measurement of silver nanoparticles. Anal. Bioanal. Chem. 409, 6027–6039. https://doi.org/10.1007/s00216-017-0530-4.

Lockwood, T.E., Gonzalez de Vega, R., Clases, D., 2021. An interactive Python-based data processing platform for single particle and single cell ICP-MS. J. Anal. At. Spectrom. 10, 1039. https://doi.org/10.1039/d1ja00297j. D1JA00297J.

Mason, R.P., 2013. Trace Metals in Aquatic Systems: Mason/Trace Metals in Aquatic Systems. John Wiley & Sons, Ltd, Chichester, UK. https://doi.org/10.1002/9781118274576.

Meermann, B., Nischwitz, V., 2018. ICP-MS for the analysis at the nanoscale – a tutorial review. J. Anal. At. Spectrom. 33, 1432–1468. https://doi.org/10.1039/c8ja00037a.

Montaño, M.D., Olesik, J.W., Barber, A.G., Challis, K., Ranville, J.F., 2016. Single Particle ICP-MS: advances toward routine analysis of nanomaterials. Anal. Bioanal. Chem. 408, 5053–5074. https://doi.org/10.1007/s00216-016-9676-8.

Montaño, M.D., von der Kammer, F., Cuss, C.W., Ranville, J.F., 2019. Opportunities for examining the natural nanogeochemical environment using recent advances in nanoparticle analysis. J. Anal. At. Spectrom. 34, 1768–1772. https://doi.org/10.1039/c9ja00168a.

Montaño, M.D., Cuss, C.W., Holliday, H.M., Javed, M.B., Shotyk, W., Sobocinski, K.L., et al., 2022. Exploring nanogeochemical environments: new insights from single particle ICP-TOFMS and AF4-ICPMS. ACS Earth Space Chem 6, 943–952. https://doi.org/10.1021/acsearthspacechem.1c00350.

Ohnemus, D.C., Torrie, R., Twining, B.S., 2019. Exposing the Distributions and Elemental Associations of Scavenged Particulate Phases in the Ocean Using Basin-Scale Multi-

Element Data Sets. Global Biogeochem. Cycles 33, 725–748. https://doi.org/10.1029/2018gb006145.
Olesik, J.W., Gray, P.J., 2012. Considerations for measurement of individual nanoparticles or microparticles by ICP-MS: determination of the number of particles and the analyte mass in each particle. J. Anal. At. Spectrom. 27, 1143–1155. https://doi.org/10.1039/C2JA30073G.
Pace, H.E., Rogers, N.J., Jarolimek, C., Coleman, V.A., Higgins, C.P., Ranville, J.F., 2011. Determining transport efficiency for the purpose of counting and sizing nanoparticles via single particle inductively coupled plasma mass spectrometry. Anal. Chem. 83, 9361–9369. https://doi.org/10.1021/ac201952t.
Rand, L.N., 2019. Using single particle ICP-MS to study occurrence and behavior of engineered, natural, and incidental nanoparticles in freshwater streams.
Rand, L.N., Ranville, J.F., 2019. Characteristics and stability of incidental iron oxide nanoparticles during remediation of a mining-impacted stream. Environ. Sci. Technol. 53, 11214–11222. https://doi.org/10.1021/acs.est.9b03036.
Rand, L.N., Flores, K., Sharma, N., Gardea-Torresdey, J., Westerhoff, P., 2021. Quantifying nanoparticle associated Ti, Ce, Au, and Pd occurrence in 35 U.S. Surface waters. ACS EST Water 1, 2242–2250. https://doi.org/10.1021/acsestwater.1c00206.
Rodushkin, I., Nordlund, P., Engström, E., Baxter, D.C., 2005. Improved multi-elemental analyses by inductively coupled plasma-sector field mass spectrometry through methane addition to the plasma. J. Anal. At. Spectrom. 20, 1250. https://doi.org/10.1039/b507886e.
Rygg, Brage, 2008. Dyrelivet På Bunnen Av Førdefjorden Og Bunnsedimentenes Sammensetning. Norsk institutt for vannforskning (NIVA).
Sanchís, J., Jiménez-Lamana, J., Abad, E., Szpunar, J., Farré, M., 2020. Occurrence of cerium-, titanium-, and silver-bearing nanoparticles in the Besòs and ebro rivers. Environ. Sci. Technol. 54, 3969–3978. https://doi.org/10.1021/acs.est.9b05996.
Simonsen, M., Teien, H.-C., Lind, O.C., Saetra, Ø., Albretsen, J., Salbu, B., 2019. Modeling key processes affecting Al speciation and transport in estuaries. Sci. Total Environ. 687, 1147–1163. https://doi.org/10.1016/j.scitotenv.2019.05.318.
Skei, J.M., Melsom, S., 1982. Seasonal and vertical variations in the chemical composition of suspended particulate matter in an oxygen-deficient fjord. Estuar. Coast Shelf Sci. 14, 61. https://doi.org/10.1016/s0302-3524(82)80067-4. IN1.
Staalstrøm, A., Molvær, J., 2009. Spredning Av Partikler I Overflatelaget Utenfor Engebøfjellet. Norsk institutt for vannforskning (NIVA).
Stolpe, B., Hassellöv, M., 2010. Nanofibrils and other colloidal biopolymers binding trace elements in coastal seawater: significance for variations in element size distributions. Limnol. Oceanogr. 55, 187–202. https://doi.org/10.4319/lo.2010.55.1.0187.
Stumm, W., Morgan, J.J., 1996. Aquatic Chemistry: Chemical Equilibria and Rates in Natural Waters, third ed. Wiley, New York.
Sturgeon, R., Berman, S.S., Kremling, K., 1987. Sampling and storage of natural water for trace metals. CRC Crit. Rev. Anal. Chem. 18, 209–244. https://doi.org/10.1080/10408348708542804.
Taylor, H.E., 2001. Inductively Coupled Plasma-Mass Spectrometry. Academic Press.
Timerbaev, A.R., Kuznetsova, O.V., Keppler, B.K., 2021. Current trends and challenges in analysis and characterization of engineered nanoparticles in seawater. Talanta 226, 122201. https://doi.org/10.1016/j.talanta.2021.122201.
Toncelli, C., Mylona, K., Tsapakis, M., Pergantis, S.A., 2016. Flow injection with on-line dilution and single particle inductively coupled plasma – mass spectrometry for monitoring silver nanoparticles in seawater and in marine microorganisms. J. Anal. At. Spectrom. 31, 1430–1439. https://doi.org/10.1039/c6ja00011h.
Vidmar, J., Buerki-Thurnherr, T., Loeschner, K., 2018. Comparison of the suitability of alkaline or enzymatic sample pre-treatment for characterization of silver nanoparticles in human tissue by single particle ICP-MS. J. Anal. At. Spectrom. 33, 752–761. https://doi.org/10.1039/c7ja00402h.
Vidmar, J., Hässmann, L., Loeschner, K., 2021. Single-particle ICP–MS as a screening technique for the presence of potential inorganic nanoparticles in food. J. Agric. Food Chem. 69, 9979–9990. https://doi.org/10.1021/acs.jafc.0c07363.
von der Heyden, B.P., Hauser, E.J., Mishra, B., Martinez, G.A., Bowie, A.R., Tyliszczak, T., et al., 2014. Ubiquitous presence of Fe(II) in aquatic colloids and its association with organic carbon. Environ. Sci. Technol. Lett. 1, 387–392. https://doi.org/10.1021/ez500164v.
Waegeneers, N., De Vos, S., Verleysen, E., Ruttens, A., Mast, J., 2019. Estimation of the uncertainties related to the measurement of the size and quantities of individual silver nanoparticles in confectionery. Materials 12, 2677. https://doi.org/10.3390/ma12172677.
Wells, M.L., 2002. Marine colloids and trace metals. In: Biogeochemistry of Marine Dissolved Organic Matter. Elsevier, pp. 367–404. https://doi.org/10.1016/B978-012323841-2/50009-9.
Wells, M.L., Goldberg, E.D., 1992. Marine submicron particles. Mar. Chem. 40, 5–18. https://doi.org/10.1016/0304-4203(92)90045-c.
Westbroek, P., De Jong, E.W., van der Wal, P., Borman, A.H., 1984. Mechanism of calcification in the marine alga *Emiliania huxleyi*. Phil. Trans. Roy. Soc. Lond. B 304, 435–444. https://doi.org/10.1098/rstb.1984.0037.
Wilkinson, K.J., Lead, J.R., 2007. Environmental Colloids and Particles: Behaviour, Separation and Characterisation. John Wiley & Sons, Ltd.
Bruvold, Are Sæle, 2023. Raw SP-ICP-MS data for the publication "Vertical distribution of inorganic nanoparticles in a Norwegian fjord". https://doi.org/10.5281/zenodo.6187221.